PHOTOINDUCED IRREVERSIBLE EFFECTS ON MAGNETIC PROPERTIES AND ALLIED PHENOMENA IN MAGNETIC OXIDES XII

[Review]

[a] K. Hisatake, I. Matsubara, K. Maeda, T. Fujiwara, M.Peters

[b]S.Abe, K.Kudo, [c]S. Kainuma, [d] C. de Francisco, J. M. Muñoz , P. Hernández,

O. Alejos. C.Torres

[a]Faculty of Dentistry, Kanagawa Dental College, Kanagawa 238-8580, Japan

[b]Faculty of Engineering, Kanagawa University, Yokohama 221-8686, Japan

[c]Faculty of Engineering, Ashikaga Institute of Technology, Tochigi 326-8558, Japan

[d]Facultad de Ciencias, Universidad de Valladolid, Valladolid E-47071, Spain

A review is presented of the various experimental results that have thus far been developed for the study of disaccommodation(DA) in a single crystals of yttrium iron garnet, which is irradiated with laser (the most effective wavelength is 700 nm) or white light at 77 K. And these results are limited to development in our laboratories, although the important contribution by many researchers cannot be excluded to the phenomena. Then, a remarkable change of the temperature dependence of complex permeabilities μ'' and is observed, which is specific to photoinduced magnetic effect. New results of dark disaccommodation are also described in relation to loading impact, which is as yet not published. These origin has been discussed on the basis of new concept, that is, photoinduced structure change.

1.1 Introduction

The understanding of interaction of light-magnetism in highly excited soft magnetic materials is important not only in basic research but also for their application as optical devices. A microscopic description is quite complicated due to the interference of various aspects. The electrons and holes form a many-particle system interacting with each other via Coulomb forces as well as with lattice and impurities. Intense light fields drive the system into nonequilibrium. In $Y_3Fe_3O_{12}$ (YIG) containing Si^{4+}-Fe^{2+} center with a small concentration, changes of magnetic properties by irradiation (photomagnetic effects, denoted here by photoinduced magnetic effect ,PME have been found and classified into two types. Teale and Temple[1] observed for a concentration of 0.1 Fe^{2+} molecule the growth of a uniaxial anisotropy at 20 K in the magnetization direction by irradiation of a magnetically saturated crystal. This phenomenon was attributed to a redistribution of the ferrous ions among the four kinds of octahedral sites in which the ferrous ions have a uniaxial anisotropy with the easy axis along one of the four cubic (111) directions. Such PE depending on the magnetization state have been called "type I" effect, Enz, van der Heide, Metselaar and Rijnierse[2] found on a sample having a lower Fe^{2+}, concentration (=0• 005 Fe^{2+}in molecule) a permeability decrease from 120 down to 20 in about 2 sec by irradiation of a polycrystalline sample at 77 K and it was observed to be irrelevant whether the material was in the saturated or in the demagnetized state during irradiation. The effect was attributed to a photo-induced excitation of weakly anisotropic Fe^{3+} ions trapped around Si^{4+}ions (Fe^{2+} type I) to "ideal" lattice sites far from Si^{4+} ions or other

lattice imperfections (Fe^{2+} type II). The behavior can.then be explained by assuming that the Fe^{2+}(II) ions are strongly anisotropic, immlobile and distributed at, random among the octahedral sites. The concentration fluctuations of the hard ions result in pinning of domain walls that can account for the decrease as observed. Such a PME indepcndent of the magnetization state has been classified as a "type II" effect. The type I effect described above has been attributed to a redistribution of Fe^{2+}(I) ions under the assumption that the radiation absotption depends on the angle. During irradiation the four types of octahedral sites are non-equivalent so that the redistribution results in a selective occupation depending on the rnagnetization direction. The interpretation given above is essentially based on the assumption that a Fe^{2+} ion is located on a certain lattice site. Potential barriers hinder Fe^{2+} from hopping so that the PME cannot be wiped out by thermal Fe^{2+} diffusion (relaxation). The wipe-out process is found to start at about 150 K and is over in a few seconds at 230 K. The starting point of the present work has the consideration that a replacement of Fe^{2+} by another strongly anisotropic process, for instance like phtoinduced lattice distortion may bring the fixation of photoinduced magnetic effects by making relaxation to the original state more difficult. On the other hand, the induced preferred directions within the domain wall in soft materials create localized potential minima. As these minima become deeper with time, the mobility of the domain wall will decrease. The gradual decrease after demagnetization or magnetic slow relaxation of initial permeability μ_i is called the disaccommodation (DA). On the other hand, photoinduced disaccommodation is termed as PDA[3]. In this report, we review the experimental results of PDA, in not Si- but Ca-doped YIG[4,5] and a clue to explain why it is possible for the single or double peaks of PDA[5] to exist in YIG single crystal. These effects are completely reversible by the irradiation–annealing cycle. In the following section, we treat generally time-dependent magnetization processes. These processes become particularly important when the magnetization must change rapidly, as in mechanical shock or pulsed fields.

1.2 Magnetic after effects

1.2.1 General remarks

Magnetic after-effect is defined as the phenomenon in which a change in magnetization is partly delayed after the application of a magnetic field[6]. This phenomenon is sometimes referred to as magnetic viscosity. Eddy currents may cause a delay in magnetization, but this kind of purely electrical phenomenon is regarded here as different from magnetic after-effect. Magnetization may also be affected by purely metallurgical phenomena such as precipitation, diffusion, or crystal phase transition; this kind of magnetization change is also excluded from the definition of magnetic after-effect. Structural changes like those in the previous sentence, if they occur slowly at or near room temperature, are usually known as aging. The difference between magnetic after-effect and magnetization changes due to aging is that changes resulting from magnetic after-effect can be erased by application of an appropriate magnetic field, while changes due to aging are not recoverable by purely magnetic means. Suppose that a magnetic field $H = H_1$ is applied to a magnetic material, and is suddenly changed to $H = H_2$ at $t = 0$. There is an immediate change in magnetization, I_i, but there is an additional change, I_n, occurring over time. The time varying part I_n can be written generally as

$$I_n = I_n(t). \qquad (1.2.1)$$

The magnitude of I_n is a function of I_i and also depends on the final magnetic state at H_2. For example, if the final state is in the field range for magnetization rotation, the value of I_n is very small, while if the final state is in a field range for irreversible magnetization, such as near the residual magnetization or the coercive field, I_n may be fairly large. In the simplest case, $I_n(t)$ can be expressed by a single relaxation time τ to give

$$I_n(t) = I_{n0}\{1 - \exp(t/\tau)\}, \qquad (1.2.2)$$

where I_{n0} is the total change in magnetization from $t = 0$ to infinity, not including I_i .being negligibly small. The magnetic after-effect also causes a delay in magnetization in a material subjected to an AC magnetic field. In order to express this phenomenon mathematically, we consider a differential equation which leads to (1.2.2) for DC magnetization. Suppose that an AC magnetic field expressed as

$$H = H_0 \exp(i\omega t) \qquad (1.2.3)$$

is applied to a magnetic material. Then changes in magnetization are delayed so that

$$I = I_0 \exp i(\omega t - \delta) \qquad (1.2.4)$$

where δ is the delay expressed as a phase angle. In order to find the angle δ and the amplitude I_0, we use (1.2.2) and (1.2.3) in (1.2.4). Then we find

$$\tan \delta = \zeta\omega\tau / \{(1 + \zeta) + (\omega\tau)^2\} \qquad (1.2.5)$$

Since the appearance of a nonzero angle δ results in a power loss, we call this angle δ the loss angle and tan δ the loss factor. For YIG, we observed this behavior and reported it, so long as temperature dependence of the loss factor, tan δ, observed for a low carbon iron is often cited. The numerical values are the frequencies of the AC field in hertz. The curve shows one or two maxima at some temperatures, because the relaxation time τ varies with temperature. If we consider (1.2.5) to be a function of τ, tan δ becomes very small for large τ, because the denominator increases as τ^2, while the numerator increases only as τ. For small τ, tan δ becomes also small, because the numerator becomes small, while the denominator stays almost constant. The maximum occurs for

$$\tau = (1+\zeta)^{1/2} / \omega \qquad (1.2.6)$$

determine the relaxation time from the angular frequency of the maximum at a particular temperature. We see that both groups of experimental points fall on the same straight line, which means that both phenomena have the same origin. In order to understand the nature of this phenomenon, a model proposed by Snoek is helpful[6]. Suppose a heavy ball is placed on a concave surface covered with a layer of thick mud. If the ball is displaced by a lateral force H, it will sink gradually into the layer of mud, changing its equilibrium position. This corresponds to the semistatic magnetic after-effect. AC magnetization corresponds to the case when the ball is oscillating back and forth around the minimum position of the concave surface under the action of an alternating force. As the viscosity of mud increases at low temperatures, the ball will move on the hard mud surface with very low loss. On the other hand, when the viscosity decreases at high temperatures, the ball will move through a low-viscosity mud layer, resting on the concave surface, again resulting in very low, Ioss. At an intermediate temperature, the motion of the ball is most severely damped, and a very large loss results. This is the reason why the loss factor has a maximu:m at an intermediate temperature. The magnetic after-effect is not necessarily described by a single relaxation time. In general the relaxation times are distributed over some finite range. If the relaxation times are distributed over a wide range, we can conveniently use In T as a parameter instead of T. Let the volume in which the logarithm of the relaxation time is in the range In T to In T+d(In T) be g(T)d(In T). Since g(T)d(In T)={g(T)/T}dT, the distribution function g(T) can be normalized by

$$\int_0^{\infty} \frac{g(\tau)}{\tau} d\tau = 1 . \qquad (1.2.7)$$

Then the time change of magmetization can be described by

$$I_n(t)=I_{n0}\left(1- \int_0^{\infty} \frac{g(\tau)}{\tau} \exp(-t/\tau) d\tau\right) . \qquad (1.2.8)$$

If we assume for simplicity that the distribution function is a constant g from τ_1 and τ_2 and zero out side this range , We have from (1.7),

$$g=1/\ln(\tau_2/\tau_1), \qquad (1.2.9)$$

for $\tau_1 < \tau < \tau_2$. If we put $t/\tau = y$, the second term of (1.8) becomes

$$\Delta I_n = I_{n0} - I_n = \{ I_{n0} / \ln(t_2/t_1) \} \int_{\tau_1}^{\tau_2} \frac{1}{\tau} \exp(-t/\tau) d\tau$$

$$= \{ I_{n0} / \ln(t_2/t_1) \} \int_{t\tau_2^{-1}}^{t\tau_1^{-1}} \exp(-y)/y dy \qquad (1.2.10)$$

If we set

$$N(\alpha) = \int_{\alpha}^{\infty} \frac{1}{y} \exp(-y)/dy , \qquad (1.2.11)$$

(1.2.10) can be expressed as

$$\Delta I_n = \{ I_{n0} / \ln(\tau_2/\tau_1) \} \{ N(t/\tau_2) - N(t/\tau_1) \}. \qquad (1.2.12)$$

The function $N(\alpha)$ is expressed approximately by

For $\alpha \ll 1$ $\quad N(\alpha) = -0.577 - \ln \alpha + \alpha - \alpha^2/2 \cdot 2! + \alpha^3/3 \cdot 3! +$

for $\alpha \gg 1$ $\quad N(\alpha) = e^{-\alpha}/\alpha - 1!/\alpha + 2!/\alpha^2 - \cdots$

for $\alpha \gg 1$ $\quad N(1) = 0.219$

The physical mechanism of the magnetic after-effect was proposed by Snoek[6] and later corrected by Neel.[6] The carbon or nitrogen atoms, which are very small compared with an iron atom, occupy interstitial sites in the body-centered lattice of iron. There are three kinds of interstitial sites, identified as x-, y-, and z-sites[7]. If many carbon atoms occupy x-sites preferentially, the pseudodipolar interaction of the Fe-Fe pairs in the x-direction is changed, thus inducing a uniaxial magnetic anisotropy.

1.3 Point defects in YIG contributing to an induced anisotropy

1.3.1 Electronic properties of point defects ; the F-Center

The F center, an electron trapped at an anion vacancy is the best-understood point defect in ionic crystals. Indeed, because of the range of systems and processes for which it is characterized in detail, it is common color centers in alkali halides MX[8]. These include electron-excess centers, notably the F center and related defects (the F' center has an extra electron; the FA center is an F center with an adjacent cation impurity; the F_2 center is two adjacent F centers), and two centers involving X_2 molecular ions, namely, the self-trapped hole (V_K center) and neutral anion interstitial (H center). The F center, with a single electron localized by the net positive charge of the missing anion, has obvious analogies with the hydrogen atom. These can be exploited in several ways. First, one can label states in the same way, referring to the 1 s, 2s, states. This needs slight generalization, because of lattice relaxation. Thus it is usual to use the convention for the state reached by a Franck-Condon transition (constant lattice geometry) from the 1 s ground state; the corresponding state following lattice relaxation in the vicinity of the excited F center is referred to as 2p. A second use of the analogy is to give rough estimates of transition energy and orbital radius. A simple change of dielectric constant gives for the energy of the 1s→2p transition of the F-center (F band), the energy of the corresponding transition in the hydrogen atom. Ignoring the change in effective mass of the F electron leads to an effective radius of a bohr radii. Third, most calculations on f centers use a variational method, guessing a physically reasonable wavefunction, and minimizing the energy with respect to a variational parameter a. Hydrogen atom wave functions scaled in the manner mentioned above are indeed quite a good starting point for a trial function. It is found experimentally for F-band absorption (but not emission) that the relation as holds quite well for alkali halides where a is the cation-anion spacing measured in angstrom units. It suggests strongly that the dominant energies depend only on lattice geometry. This can only occur if the point-ion potential dominates, that is, if one can replace anions and cations by point charges. Indeed, the point-ion model proves a very respectable and successful approximate description. It does have its limitations, and these are conveniently estimated as ion-size corrections in the pseudo-potential formulation. Continuing the analogy between the F center and the hydrogen atom we expect an infinite series of excited levels of the F center converging on a continuum, in this case the ionized states with the electron delocalized in the conduction band. A relatively weak asymmetric absorption band tailing to high energy occurs on the high-energy side of the F-band . This band, which has about 10% of the strength of the F band, is referred to as the K band; it consists of a superposition of transitions is 3p→np. There is a high quantum efficiency for photoconductivity associated with excitation in the high-energy tail of the K band. Still weaker absorption bands of the F center, called the L bands, occur a few eV higher in energy than the K band and have an intensity of -1% of the F-band intensity. Excitation in these bands gives photoconductivity with a higher quantum efficiency than in the K band, and there seems little doubt that the L bands are conduction-band states perturbed by the F center[8]. The luminescence of F centers raises two important points. First, does one expect to see luminescence at all. The second point concerns the F-center lifetime. Measurement of the oscillator strength of the F -band in absorption and application of the principle of detailed balance suggests that the luminescence of the F center in KCl, assuming a transition, should have a lifetime of ~ 10^{-8} sec and a quantum efficiency near unity. This fact suggests the long life time of PME at the low temperatures. The F center in halides is electrically neutral. However, it may lose its electron forming an empty anion vacancy (the a center) or gain another electron forming a charged center (the F' only at low temperatures) and have a broad absorption band going through the visible region, usually at lower energies than F-band itself. The center gives rise to an absorption β and in the ultraviolet; in KI, for example, the F-β and occurs at 238 nm, close to the first exciton peak, at 230 nm. It is generally assumed that this band is due to creation of a perturbed exciton near the ionized F center[9,10]. A perturbed exciton band associated with the (neutral) F center, the so-called b band, occurs between the a band and the first exciton peak of the perfect crystal. In oxides an oxygen vacancy may trap a single electron forming the F center, resembles the F center in halides. In addition, the oxygen vacancy readily traps two electrons forming the F' center (occasionally misleadingly written as F center) and this corresponds to the two-electron F' center in halides. Color-center

systems have been operated as infrared lasers, broadly tunable in the range 0.4-1eV (depending on host and center) and capable of continuous operation. The color centers involved are all related to the F center. One might expect a close parallel in ionic solids between trapped electron centers and trapped hole centers, for example, one might expect to find the antimorph of the F center where a cation vacancy traps a hole, giving the V center in halides or the V center in oxides. However, the difference between electron and hole centers are more striking than the parallels. In halides the V center is relatively hard to produce, and has not been intensively studied. In oxides, however, the V center is one of the most studied intrinsic defects. The cation vacancy in MgO with a single trapped hole (i.e., an MgO crystal from which Mg has partly been removed) has an effective single negative charge in the crystal and is an example of a V center. Similar centers occur in GaO, SrO, and BaO, in the fourfold coordinated oxides like BeO and ZnO, and in related sulfides, selenides, and tellurides. The V center readily associates with other defects, for example, substitutional Al and easily captures hydrogen or alkali ions; it may also capture another hole to form the neutral V. The V center has been studied extensively by EPR and optical methods. The results show dramatic differences from the F- center in the same host. First, EPR spectra at low temperatures demonstrate that the hole is localized on a single neighboring oxygen ion, so that in MgO there are one O and five O^{2-} ions next to the magnesium vacancy. As the temperature rises the hole moves more and more rapidly among the equivalent oxygens until it appears delocalized at room temperature. These experiments and concepts suggest the model of PMD. Second, there are two types of optical transition. One consists of transitions internal to the O ion on which the hole is localized (the so-called crystal-field transitions, since the transition energy is determined almost entirely by the electrical field at the O ion caused by the absence of Mg. The other, more important, transitions are the charge transfer type in which the hole moves to other neighbors of the vacancy. Similar charge transfers are important in determining the color of gem-stones and in donor-acceptor pair recombination. Why is the hole initially localized on one oxygen ? If it were delocalized, forming bandlike states over all six neighbors, without asym-metric distortion, there would be an energy gain. This gain competes with possible gains in polarization energy associated with charge localization. The predicted energies, in eV, refer to the charge-transfer calculations unless otherwise stated. We can illustrate this latter effect by supposing that a charge q is divided into N portions, placed far apart in a polarizable crystal. For each charge the polarization energy is proportional to the square of the charge. The N fractional charges have polarization energy gain that is, so that polarization always favors localization. Both detailed qualitative analysis and accurate quantitative estimates agree that for a hole trapped by a cation vacancy the polarization terms win, giving localization. For a free hole in an otherwise perfect crystal the balance is marginal, but delocalized holes in oxides tend to be generally more stable by a few tenths of one eV. Exactly the same polarization terms and similar but not identical tunneling terms enter in the charge-transfer energy. The initial and final oxygens involved in the charge-transfer transitions are exactly equivalent apart from distortion and polarization; the charge-transfer energy between such equivalent ions would be zero in an unrelaxed, unpolarized host. Charge transfer can occur at more than one transfer range. It is a general rule that the longer the range the weaker the transition and the higher its energy. This may also be related to the phootoinduced magnetic effects.

1.3.2 Persistent photoconductivity in non-magnetic oxide films as a method of photodoping ;comparison between photoinduced magnetic effect and conductive effect

It is well known that high-temperature superconductivity arises from doping of parent metal-oxide semiconductor compounds in the immediate vicinity of the semiconductor-to-metal transition. Resistive properties of $YBa_2Cu_3O_{6\pm x}$ can be changed easily over a wide range, from dielectric to metallic, by varying the oxygen concentration within the limits of $0 < x < 1$[16]. The unit cell of this compound contains CuO_2 double planes, responsible for the superconducting properties, and CuO- layers with the oxygen concentration being variable. $YBa_2Cu_3O_6$ (x =0) is a dielectric antiferromagnet with a tetragonal crystal lattice. of x, in the CuO~

layers results in an increase of the free-carrier concentration (holes) in the CuO_2 double layers. The exposure dose of the samples was increased, a transition from the semiconducting to a metallic state occurred. As evidenced by simultaneous measurements of conductivity and magnetic properties of the films irradiated at 5 K, metastable photoinduced superconductivity was developed and enhanced with increasing exposure time. illuminated films showed at room temperature only very slow relaxation of the photoinduced conductivity (relaxation time being of the order of 10 h) toward the equilibrium value. After accomplishing the relaxation at temperatures of 300-320 K, the transport properties of the films were restored to those before irradiation. This experimental results are very similar to our experiments, in spite of existence of the fundamental difference between the ferromagnetic and non magnetic substance. The photoinduced enhancement of superconductivity in $YBa_2Cu_3O_{6+x}$ films has been confirmed in recent experiments. It was suggested under irradiation of these films, the concentration of free holes is increased (photodoping), leading to similar effects in transport and magnetic properties as would result from increasing of the oxygen contents of the sample. Photoconductivity can be regarded as an alternative method of doping semiconductors, the number of free carriers remains relatively small. However, superconductivity of the HTSC compounds shows up most vividly in the intermediate vicinity of the semiconductor-to-metal tran-sition. Therefore it can be expected that even a small increase of carrier concentration by photodoping will initiate or enhance their superconductivity. The conductivity by 10^{-11} orders or magnitude over that in the unexposed state has been reported. Apart from transient photoconductivity, a number of semiconductors exhibit persistent photoconductivity illuminated films showed at room temperature only very slow relaxation of the photoinduced conductivity (relaxation time being of the order of 10 h) toward the equilibrium value. After accomplishing the relaxation at temperatures of 300-320 K, the transport properties of the films were restored to those before irradiation. The photoinduced enhancement of superconductivity in $YBa_2Cu_3O_6$ films has been confirmed in recent experiments. It was suggested under irradiation of these types of the films, the concentration of free holes is in-creased (photodoping), leading to similar effects in transport and magnetic properties as would result from increasing of the oxygen contents of the sample. Experimental evidence for the PPC and related photoinduced phenomena have been reported in short communications.

1.3.3 Oxygen ordering in the YBCuO sample

The semiconductor-to-metal transition in $YBa_2Cu_3O_{6+x}$ is assumed to result from charge transfer from CuO_2 planes to the Cu-O-Cu- chains in the CuO-layers. The p orbitals of O ions in the chains are partially filled and there exist a great number of acceptor centers (localized holes) formed by the unoccupied p orbitals of O. At low oxygen content (x ~0.2), only one oxygen ion appears in a divalent state, O^{2-}, and the other (n -1) oxygen atoms are transformed into the 0 states with simultaneous ionization of (n +1)Cu+ ions into a Cu state. Thus there are n -1 holes in the p orbitals of O ions belonging to a n-mer chain frag-ment. When x is increased in the CuO- layers, the concentration of the chain fragments and their average lengths grow. At x ~0. 4 the average chain length exceeds the critical value and it becomes energetically favorable to transfer electrons from CuO_2 planes to the CuO- layers, inducing thereby hole conductivity in the CuO_2 planes. At the same time, the chain fragments are arranged predominantly along the b axis and the tetragonal to orthorhombic phase transition occurs. The local oxygen structure in an O-deficient sample depends strongly on the annealing procedure, and a number of metastable phases have been observed. The oxygen ordering can occur in domains at low x may be of very small size . With a certain probability, the electron transfer to an adjacent CuO- layer where it is trapped in unoccupied p levels of O, localized deep in the gap (- 1.8 eV) between the valence and upper excited bands. The photoexcited holes gradually increase the total concentration of free holes in CuO_2 planes, and the film changes from semiconducting to metallic (photodoping). If the concentration of the free carriers corresponds before exposure to the onset of the SC phase, photodoping would lead not only to an increase of the conductivity, but also to growth of the SC phase. For T <270 K, the photoexcited electron trapped at O is

unable to overcome the barrier. This is why no relaxation of the photoconductivity (and photoinduced supercon-ductivity) is observed in this temperature range. At room temperature the relaxation of PPC is possible by thermal excitation of the trapped electrons over the barrier to the upper conduction band. Inhomogeneity of the oxygen concentration gives rise to some distribution of the trap levels, explaining the reason for the stretched-exponential growth and decay of PPC. In the framework of the above mechanism, the relaxation parameter A(x) can be considered as the energy difference between localized oxygen.

1.3.4 Deep level centers correlated with our experiment

Deep level centers are connected to conduction and valence bands and often provide a preferred path for carrier recombination or act as deep traps. In general, deep level centers require a tight-binding analysis in which, at least for the ground state, the wave function remains localized close to the core of the defect. They cannot be described by a hydrogenic effective mass approximation. Deep levels, however, do not necessarily require a large binding energy. They are connected to the conduction and valence bands, i.e., these deep trap levels do not follow one specific band when perturbed by alloying or the application of hydrostatic pressure. Their central core potential dominates their behavior at the ground state, or they have unsaturated inner shells in transition metal impurities, permitting electronic transitions here. Specifically, such defects may or may not be charged relative to the lattice; they may be isoelectronic or isovalent. The levels of these centers are described by a short-range potential. The pseudopotential method is an advantageous tool for determining V(r). In addition, the deformed lattice environment must be considered and for Jahn-Teller distortion[10]. The deep states extend throughout the entire Brillouin zone. States from both bands and all near-band gap valleys are necessary to construct the ground-state electron eigenfunction of this center. The resulting deep defect levels communicate with both bands and act as deep traps for electrons or holes or as recombination centers. A new review of such deep centers; persistent photoconductivity and photoionization of deep electron traps can be found by K.Sato[11]. Strong persistent photoconductivity (PPC) has been observed in bulk n-type CdMnTe crystals heavily doped with Ga at low temperatures (below 150 K). The kinetics of the PPC effect were investigated by means of photoconductivity and photo-Hall measurements. The observed photoconductivity transients displayed a strongly nonexponential behavior. We use the observed transient behavior to show that the transfer of electrons from the ground state of defects, responsible for the PPC, to the conduction band proceeds in two steps, via an intermediate state of the defects. Numerical simulations based on the two-step photoionization model are in excellent agreement with the experimental data. From a detailed analysis of the spectral and temperature dependence of the carrier-concentration transients and of the photo-Hall data, we establish that the transition from the ground to the intermediate state is not accompanied by electron emission, i.e., the defect remains in the same charge state. The analysis of the spectral and temperature dependence of the photoionization cross sections indicates that both states of the defect are strongly coupled to lattice vibrations, and the large lattice relaxation mechanism is recognized as the mechanism responsible for the metastability of the free carriers leading to the observed PPC. No magnetic-field effect on photoemission has been observed, indicating that effects associated with deep levels are insensitive to the above exchange interaction. Persistent photoconductivity (PPC) [12] is a property exhibited by certain semiconductors, where the exposure of the material to light at sufficiently low temperatures results in an increase of the carrier concentration that persists for a very long time (of the order of minutes to years) after the irradiation is terminated. PPC has been observed in a large number of bulk semiconductors as well as in two-dimensional systems, and is one of the most interesting-although still not well understood-phenomena in contemporary semiconductor physics. Through the years many mechanisms have been proposed to explain the origin of PPC, but only two major interpretations have survived successive confrontations with experimental data. The first of these is based on the existence of macroscopic potential barriers in semiconductors. Such potential barriers are expected to be present at surfaces, interfaces, and around doping or composition inhomogeneities. The presence of these macroscopic

imperfections in the material creates built-in local electric fields that spatially separate the photogenerated electrons and holes and significantly decrease the recombination rate. The macroscopic barrier model is particularly suitable for describing PPC in artificially constructed semiconductor structures, such as the one just mentioned. The second mechanism for generating PPC assumes the presence of microscopic potential barriers, which occur around certain defect centers as a result of emission of carriers trapped at the defect sites. At low tempera-tures these microscopic barriers prevent the carriers from being recaptured. The most common origin of such microscopic barriers is the relaxation of the crystal lattice around the defect. In particular, it accounts for the extremely small thermally activated electron-capture cross section and the very large Stokes shift of the ionization energy which characterizes such defects. The best known defects which lead to PPC due to the large lattice relaxation are the so-called DX centers observed and extensively investigated in AlGa and in GaAs (under hydrostatic pressure). The widely accepted model of DX centers was developed by Chadi and Chang[13],;the microscopic barrier and the defect center responsible for PPC arise from the interstitial-to-substitutional motion of the defect, triggered by the photoionization of an electron trapped at the defect. The second mechanism for generating PPC assumes the presence of microscopic potential barriers, which occur around certain defect centers as a result of emission of carriers trapped at the defect sites. At low temperatures these microscopic barriers prevent the carriers from being recaptured. The most common origin of such microscopic barriers is the relaxation of the crystal lattice around the defect. This mechanism, known as the large lattice relaxation (LLR) model, was proposed by Lang et al.[14], assuming a strong coupling between the electronic and the vibrational properties of the defect centers, the LLR model readily explains most of the experimentally observed properties of the defects responsible for PPC[15]. In the second run, the sample is exposed to irradiation at low temperature before starting the warming. The irradiation is carried out with white light for about 30 mm, until the carrier concentration reaches its saturation value (i.e., until all centers were depopulated). The irradiation is then switched off, and the measurements are performed as a function of increasing temperature. For both runs, the warming rate was kept at approximately the same value of 1 K/mm in the temperature range between T=4.2~70 K and 250 K. The second experiment consisted of measuring the photoionization cross sections. We used the same experimental procedure as that described above for the photoinduced magnetic effect of permeability, but the irradiation of the sample was by white light rather than monochromatic light. To accomplish this, our cryostat was used in conjunction with a 100-W quartz halogen lamp. Colored glass band-pass filters in the region 650-1500 nm were used to cut off any second-order radiation. The power of the incident light at each wavelength was measured with a pyroelectric detector and a lock-in amplifier. The output photon flux, of the order of 10^{16} photons/cm^2 was kept constant at each wavelength with a variable attenuator in the visi-ble region, and with calibrated neutral density filters in the infrared region. A concave mirror focused the light onto the sample, with the area of the focal spot slightly larger than the area of the sample. The system beyond the output of the monochromator was enclosed in a specially constructed aluminum enclosure to prevent stray background light from reaching the sample. During the experiment, the sample was slowly cooled down to the desired temperature in darkness, in the time of the order of 5 h. After the temperature was stabilized (with the accuracy of 0.1 K), the monochromatic irradiation of the sample was switched on and the measurements begun. The increase of the photoconductivity was measured as a function of time by the same data-acquisition system as in the Hall measurements. After the measurement, the initial conditions were reestablished by heating the system to T= 240 K in order to quench the photoinduced DA or PPC. The irradiation at low temperatures significantly decreases the resistivity, making the conductivity easily measurable even at low temperatures. As long as the sample temperature is kept below T = 100 K, the permeability or the resistivity remains unchanged for many hours after termination of the irradiation. As the sample temperature decreases in darkness from room temperature, the carrier concentration decreases due to freeze-out of the electrons on the donor level, with a relatively large thermal ionization energy. The donor level occupation equilibrates rapidly (on the time scale of the measurements) and no persistent effect is observed. In order to calculate the thermal ionization energy of the donor level, we consider the standard

equilibrium Fermi-Dirac statistics, assuming that only electrons from the F-point minimum of the conduction band contribute to the transport. The relaxation process is so slow that the thermodynamic equilibrium cannot be experimentally obtained, and a metastable value of the electron concentration, higher than the equilibrium concentration, is observed. Irradiation of the sample at low temperatures transfers electrons from the deep traps to the conduction band (from which they can thermalize to shallow states), increasing the carrier concentration by many orders of magnitude (at least two orders at around T = 80 K and as can be seen from the trend of the resistivity data-considerably more at low temperatures). At these temperatures the electrons do not have sufficient thermal energy to surmount the capture barrier and to return to their deep levels, thus remaining persistently either in the conduction band or on shallow donors. Warming up the sample in the region T <80 K does not affect the carrier concentration *n*. As the temperature exceeds 80 K, however, the electrons begin to acquire sufficient thermal energy to overcome the barrier, and the free-electron concentration drops rapidly to its equilibrium value. We can see that the mobility increases with increasing temperature, and its values measured after photoionization, remain slightly higher than those measured in darkness. As the temperature reaches T= 100 K, suddenly drops and becomes equal to the dark stzte. Below T =100 K the ratio of (illumin./dark)- state is nearly equal to 2. The large increase of the electron concentration after irradiation by orders of magnitude in comparison with the corresponding small increase of the mobility by a factor of 2 allows us to use an approximation where photoinduced increase of the conductivity a is fully attributed to the increase of the free-carrier concentration in the conduction band. Using the above argument, we can treat the experimentally measured photoconductivity transients simply as the carrier-concentration transients. However, in the case of photoinduced magnetic effect , we can not always apply the situation mentioned above,which is one of the unsolved problems.

1.4 .1 Square Well Potential

A means of introducing the chemical individuality of a center is provided by assuming a rectangular one-dimensional well of depth -Vo and width 2a. A very similar approach is used to evaluate a level spectrum in two-dimensional and in Schottky barriers. The state of electron behavior is described by a solution of the Schroedinger equation,in which h is Planck's constant;

$$d^2\phi/dt^2 + k^2\phi = 0$$

$$k^2 = \frac{2m[E - V(x)]}{\hbar^2}$$

and (1.4.1)

$$\sqrt{\eta^2 + \kappa^2} = \kappa \tan(\kappa a)$$

with

$$\eta^2 = \frac{2m|V_0|}{\hbar^2}$$

Here, V(x) is used again as potential energy (eV), following the conventional use. With an ease, we can show that solutions of Eq. (1.4.1) exist for *k*-values that are solutions of the transcendental equations:

$$E_0 = \frac{\hbar^2}{2m_0}\kappa_n^2 + V_0.$$

with

n_q =1, 2,···., (1.4.2)

These solutions can be obtained graphically from the intersection of the left- and right-hand sides of Eqs. (1.4.2), shown in many text books of quantum mechanics. With discrete values of k obtained as solutions of Eq. (1.4.2), the permitted values of E inside the well are discrete and real. These are given by

$$En = \frac{h^2\pi^2}{2m_0a^2}n_q^2 + V_0.$$

with

n_q =1, 2,···., (1.4.3)

The electron restmass is used here since the electron remains close to the center and does not move through the lattice. The use of a better central cell potential V(r) of the defect in the Schroedinger equation would yield more realistic results for the deeper defect level spectrum. However, the inclusion of both valence and conduction bands into the model of deep centers is more important. In fact, it is this connection to both bands that permit the distinction between deep and shallow levels, as will be discussed in the following section. This will replace the linear relation between well depth (V_0) and the depth of the ground state with a much compressed relationship, for example, influence of an increasingly attractive potential, added to a screened Coulomb potential well with diameter 0.5 nm.

1.5.1 Coulomb Tail and Deep Center Potential

In addition to the central cell potential, we have to consider the long-range Coulomb potential of charged deep centers. The Coulomb tail determines higher excited states of these centers and renders them hydrogen-like, similar to shallow centers. Consequently, one or several deep levels are observed, followed by a series of hydrogen-like shallow levels close to the respective bands. The model potential combination of a square well and Coulomb potential describes the ground state of centers with the Coulomb potential predominating until, with increasing well depth, the short-range part of the potential becomes very large (> 1nm). The ground state of the center then shows typical deep level behavior, here calculated properly with interaction of valence and conduction bands. The atomic electronegativity can be used as an indicator for the depth of the square well representing the core potential. The most important results obtained for deep level defects cam be summarized as follows: a deep centers are connected to both valence and conduction bands: the energy of the deep level varies at least an order of magnitude less than the impurity potential; and although the short-range potential is dominating, the eigenfunctions of some of the deep level impurity centers, such as substitutional chalcogens in Si or 111-V compounds, extend well beyond nearest neighbors and do not change much with the chemistry of the impurity if incorporated at the same site . A means of introducing the chemical individuality of a center is provided by assuming a rectangular one-dimensional well of depth-Vo and width 2a. A very similar approach is used to evaluate a level spectrum in two-dimensional and in Schottky barriers .

1.5.1 Band Structure of YIG

When studying the band structure of YIG one encounters the same problems as in other transition metal oxides like, e.g., NiO. The problems are caused by the presence of the d-levels, which may form more or less localized bands. As in normal semiconductors there also are broad band-like states, namely a valence band which mainly is derived from oxygen 2p-orbitals and a conduction band derived from iron 4s-states or yttrium 5s-states. The energy gap between these broad bands is generally large in the transition metal oxides. From optical reflection

measurements on showed the presence of very strong bands with absorption coefficients as high as 9 x 10^5 cm^{-1} at 10.5 and 18.2 eV. The presence of a band near 10 eV with a high oscillator strength is confirmed by an analysis of the dispersion curves of a number of garnets . The high value of the absorption coefficient agrees with dipole allowed p → s transitions. At energies below 10 eV charge transfer transitions with smaller oscillator strengths are observed. The energetically lowest lying band is situated at 2.81-2.88 eV. In view of the high Faraday rotation and the low oscillator strength is attributed this band to the parity forbidden transition between oxygen 2p-states and iron 3d-states mainly octahedral in character. At 3.35 eV another charge .transfer transition is found and be-cause of its very low Faraday rotation and the high oscillator strength this band is assigned as a symmetry allowed transition from O(2p) → Fe(3d) states mainly tetrahedral in character. However, the possibility of Fe-Fe charge transfer cannot be excluded. This value agrees with the energy of the lowest charge transfer band. We therefore assume that the states involved in the optical transition can be identified with the valence and conduction band states. This identification implies that the n-type conduction takes place in a narrow band derived from Fe(3d)-orbitals mainly octahedral in character. If the degree of localization is high, occupied states in this band re denoted as Fe^{2+} states. Let us now consider our model further in connection with the experimental results. The half width of the charge transfer absorption band at 2.88 eV is about 0.3 eV, i.e., more than 10 times k*T*. This means that at least one of the two levels involved in this transition has to be broad. These measurements of a temperature independent Hall mobility in Si-doped YIG (n-type) was interpreted in terms of band conduction. The activation energy of 0.3 eV should in this case be the ionization energy of the charge carriers from the Si donors. On the other hand, one of the authors interpreted the observed temperature dependence of the photoinduced DA in YIG in terms of the hopping model. In this case, the mobility of oxygen vacancy assumed to be different from the effective charge , that is, double charged states. From previous investigations by the present authors on polycrystalline n-type YIG, there is evidence that the temperature dependence of the conductivity in these samples is mainly due to an ionization of the charge carriers. The activation energy was rather high, 0.56~0.9 eV, and these experiments therefore do not exclude a small activation energy of the mobility. Also for p-type samples the conduction mechanism is uncertain. For Ca or P_b doped YIG one finds an activation energy of 0.35-0.40 eV near room temperature. However, from the absorption spectrum of YIG with a lead excess more information is obtained. This absorption is due to transitions from the valence band to the P_b acceptor level. The observation of a broad structureless band, starting at about 0.6 eV or less, indicates the presence of a broad valence band. Our model seems not always the same but similar to the band model [See Appendix II].

2.1. Recent works in our laboratory

2.1.1 Photoinduced magnetic effects in bulk single-crystalline, polycrystalline and LPE films of YIG

The disaccommodation (DA), a gradual decrease of μ_i with time after demagnetisation that is often observed in soft magnetic substances, is phenomenologically similar to the II-effect.[3] However, many investigators feel DA is different from the II-effect, because the former is sensitive to demagnetisation while the latter is not[16]. This distinction is not yet definitive, since the material might be relaxing during demagnetising. In general, YIG is used in the form of bulk single crystals, epitaxially grown thin films, or poly-crystalline sintered samples, depending on the type of application. These three forms necessarily are prepared in different ways, and consequently, they differ in many physical properties, e.g., resistivity, optical absorption, lattice constant, as well as having distinctly different relaxation properties. Here we report an experimental study of the complicated μ_i –*T* curve produced by white-light or HeNe-laser-light irradiation of thick films of YIG at 77 K. We produced four forms of YIG. Two forms were bulk single-crystalline YIG, one (A) produced by the floating-zone method ($Y_3Fe_{4.9375}Ga_{0.0625}O_{12}$) and the other (B) produced by the flux method ($Y_{2.9}Pb_{0.1}Fe_{4.99}Si_{0.01}O_{12}$). The third was bulk polycrystalline YIG (C) produced by the usual sintering method

($Y_{3-2x}Ca_{2x}V_xIn_yFe_{5-(x+y)}O_{12}$; $0 \leqq x \leqq 0.6$, $0 \leqq y \leqq 0.4$). The fourth form was a single-crystalline film (D) of $Y_{2.96}La_{0.01}Pb_{0.03}Fe_5O_{12}$. Bulk samples of A, B, and C were 0.5mm thick[17].

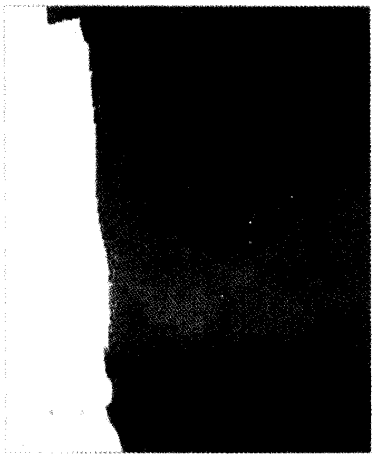

Phot.1 Sectional view of thin film ; the sample (D) through the back light.

Ring-shaped samples were approximately 0.5cm in outer diameter with a hole diameter of about 0.2cm. Energy-m(dispersive x-ray spectroscopy was used to chemically analyse samples. Unfortunately, impurities could be characterised only qualitatively because of their low concentrations. In samples of form D, the in-situ LPE method was used to deposit 13-mm single-crystalline films of YIG on both the top and bottom of a 0.5mm-thick substrate of (111) GGG. The initial permeability μ_i is a factor of ten higher than its single-crystalline counterparts. The measuring frequency and ac field are 0.2 kHz and 1 mOe, respectively. DA represents the relative change of μ_i from its initial value at time t_1 to its value at t_2, after ac-demagnetisation. DA is computed with the formula:

$$DA=\{\mu_i(t_1,T)-\mu_i(t_2,T)\}/\mu_i(t_1,T) \times 100\,(\%), \qquad (2.1.1)$$

where for an example, t_1=4sec, t_2 =8,16,24,32, 64 sec. The measurementis as follows; a sample of (A) was illuminated with either white light (~10^{16} photons/s) or a HeNe-laser ($3\cdot10^{16}$ photons/s, 633 nm) for 300s at 77 K. The sample was then allowed to warm, during which time DA was measured. We observed, confirming our previous experimental results with samples of (A) in Fig.1.5.1, two large photoinduced DA peaks centered on 125K and 210K and a small DA peak at 150K. After the sample warmed to room temperature, it was cooled to 77K. Without irradiation, it was again warmed to room temperature. No DA peaks were observed. During the entire warming process, the value of DA rose slowly from about 5 to about 20. The DA peaks were generally reproducible, although sometimes different results were obtained for different parts of the same crystal ingot. When the samples showing no photoinduced DA were sealed in a quartz tube and heated at 1300K under a reducing atmosphere for 24 hours, they showed one or two small photoinduced DA peaks. This suggests that oxygen vacancies present in the samples affect photoinduced DA. In the single-crystalline samples (B), we observed the so-called Enz-type photoinduced decrease of μ_i, 80% at 77 K, but no photoinduced DA. In one sample (x=0,y=0) selected from among the polycrystalline samples of (C) ($0 \leqq x \leqq 0.6$, $0 \leqq y \leqq 0.4$), neither Enz-type photoinduced decrease of μ_i nor photoinduced DA were observed. However, both phenomena were observed in samples with other values of x and y ($0 < x < 0.4$ and $0 < y \leqq 0.2$), although the peaks were small. One sample (x=0.1, y=0.2) was observed to have a triple-peak DA that was independent of irradiation. The

expected monotonic increase of μ_i as a function of temperature was replaced by a drastically different disaccommodation curve with double minima. Measurements of m_i in samples of (D) can be carried out readily, since its value in these samples (La~0.01 mol) is thirty times higher than that of samples containing no La[17]. The curves show the contrast between the photoinduced magnetic effect on two thin films of YIG warmed from 77 K to 300K; one was irradiated for 5 minutes at 77K, the other was not. Anomalous behavior is apparent in the upper curve, which was not irradiated at 77 K. Contrary to prediction, photoinduced quenching of DA of a sample of (D) at low temperature was also observed.

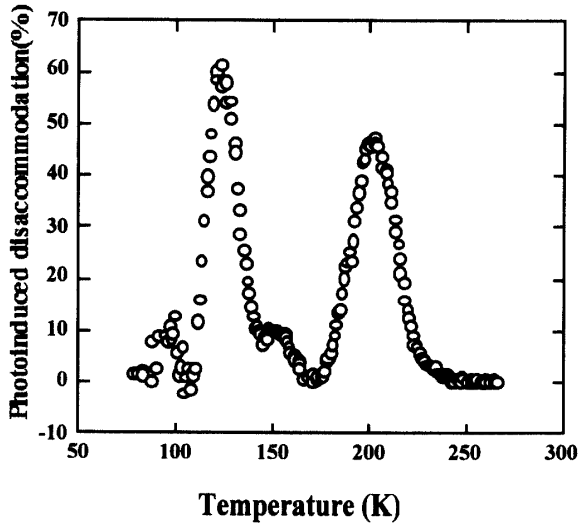

Fig.2.1.1 Temperature dependence of photoinduced DA of YIG (sample D) after white-light irradiation at 77 K.

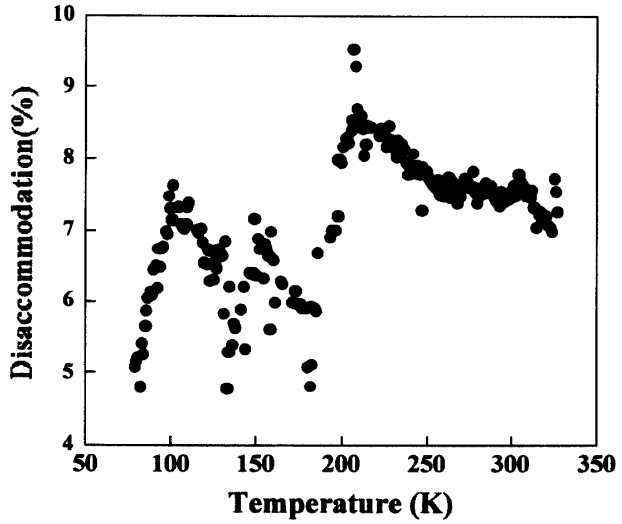

Fig.2.1.2. Temperature dependence of DA of YIG (sample B) in the dark.

At low temperature, oxygen vacancies V_o may exist even in pure crystals and behave as a type of charge reservoir that consists of one or two electrons trapped at the site and which functions as a light-sensitive injector of free electrons into the insulating system of YIG. We have tried to explain our observations of photoinduced magnetic effects on this basis, but we lack a fully adequate understanding of this problem. When electrons are excited by photons in solids, they sometimes cause a large atomic displacement. For example, a localized electronic excitation induces a large lattice distortion at any point defect, defect reaction, or structural phase transition, and this may be responsible for the Enz-type photoinduced decrease of μ_i.

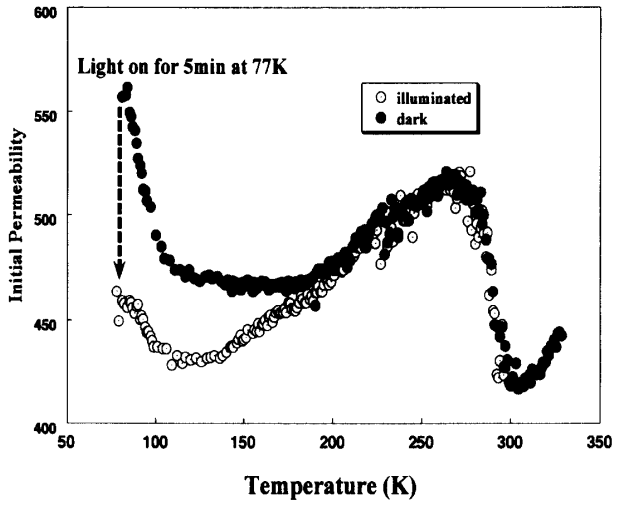

Fig.2.1.3. Temperature dependence of μ_i of the YIG thin film before and after illuminating with white light. The upper curve shows A for a samle that was not illuminated, while the curve below shows data for irradiated sample.

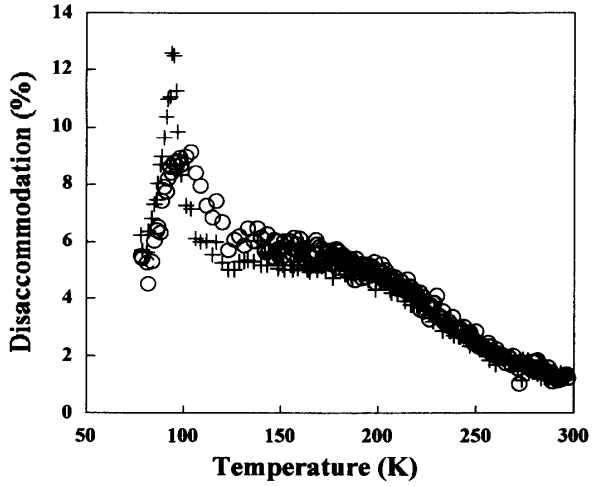

Fig.2.1.4. Temperature dependence of DA of the YIG sample (D) before and after irradiation at 77 K. + : Measured points before irradiation. O : Measured points after irradiation.

The mobility of the Fe^{2+} ion may explain why the large double DA peaks depend on temperature. After being illuminated, the strongly anisotropic Fe^{2+}, with its different binding energy, may contribute to an induced

anisotropy between an oxygen vacancy with one trapped electron and an oxygen vacancy with no trapped electrons. Generally the presence of dopants enlarges the spread of activation energies for the relaxation processes. In many cases light-induced disaccommodation processes are also found. Some results a re given for gadolinium-iron garnet and for a number of spinel ferrites. We will summarize the conclusions of the forementioned paper only briefiy. It is supposed that there occur two types of centres, labelled I and II. In the case of silicon-doped YIG the type-II centre is assumed to be an Fe ion on an octahedral site far from Si^{4+} ions, whereas the type-I center is assumed tc be an Fe^{2+} ion near the electron-donating silicon ion. So far we have discussed the off-center instability of a substitutional impurity in the off-center type self-trapping lof an exciton in alkalihalides. However, this concept can be easily also in our research field. In the ground state, two materials are different both in the chemical bonding and the lattice structure. Therefore the characters of the elementary excitations are different and have been discussed in different sections of the solid state physics. However, a local electronic excitation, which is realized by introducing of an impurity or self-trapping[10], can induces another possibility of the bonding, which is spontaneously accompanied by a symmetry breaking. In excited states of these materials, electronlc states are remixed among s- and p-orbitals of the constituents in cooperation with the atomic rearrangement. When a large atomic displacement occurs, the elementary excitations (electron, hole and the lattice) which are defmed in the starting "solid state structure lose their own meaning. There we m ust do with a more basic scheme (all valence electrons and all rons), m which we can discuss various electronic-atomic processes in all-types of s-p bonding materials. Intensive study on the atomic displacements induced by electronic excitations will present us possibility of novel structures (both local bonding and bulk structure) of the materials as well as on a deep understanding of the ground state structure.

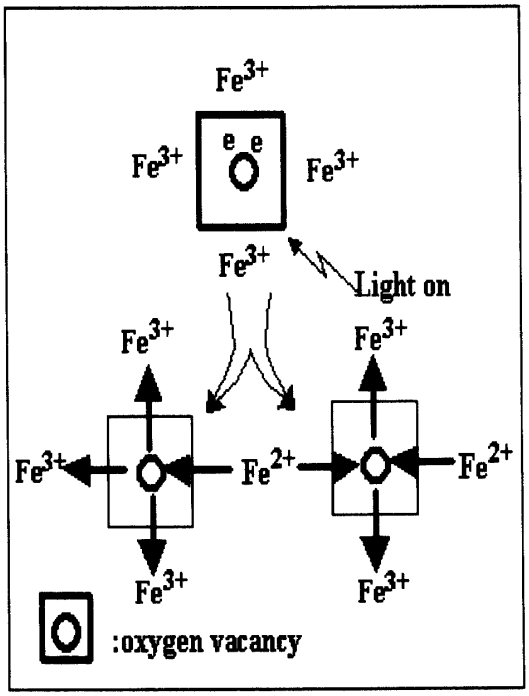

Fig.2.1.5. Two types of oxygen vacancy after irradiation. “e” represents a trapped electron near an oxygen vacancy.

2.2. Disaccommodation due to Impact loadlng

2.2.1 General remarks

Throughout this section we have considered all loading, be applied to a body in a gradual manner, such that when they reached value they remain constant or static. Some loadings, however, are dynamic; that is, they vary with time. A typical example would be caused by the collision of objects. This is called an impact loading. Specifically, impact occurs when one object strikes another, such that large forces are developed between the objects during a very short period of time. If we assume no energy is lost during impact, we can study the mechanics of impact using the conservation of energy E_c show how this is done, we will first analyze the motion of a simple block-and-spring system. When the block is released from rest, it falls a distance h, striking the spring and compressing it a distance. The fourth form was a single-crystalline film (D) of $Y_{2.96}La_{0.01}Pb_{0.03}Fe_5O_{12}$. Bulk samples of A, B, and C were 0.5mm thick. Ring-shaped samples were approximately 0.5cm in outer diameter with a hole diameter of about 0.2cm. Energy-m(dispersive x-ray spectroscopy was used to chemically analyse samples. Unfortunately, impurities could be characterised only qualitatively because of their low concentrations, before momentarily coming to rest. If we neglect the mass of the spring and assume that the spring responds elastically, then the conservation of energy requires that the energy of the falling block be transformed into stored (strain) energy in the spring; or in other words, the work done by the block's weight, falling $h + \Delta_{max}$ is equal to the work needed to displace the end of the spring by an amount D_{max}. Since the force in a spring is related to Δ_{max} by the equation $F = \Delta_{max}$ where k is the spring stiffness, then applying the conservation of energy., we have

$$U_e = U_i$$

$$W(h + \Delta_{max}) = (k\Delta_{max})\,\Delta_{max}/2$$

$$\Delta_{max}^2 - 2W\Delta_{max}/k - 2(W/k)h = 0 \qquad (2.2.1)$$

This quadratic equation may be solved for Δ_{max}. The maximum root is

$$\Delta_{max} = W/k + \{(W/k)^2 + 2(W/k)h\}^{1/2} \qquad (2.2.2)$$

If the weight W is applied statically or gradually to the spring, the end displacement of the spring is

$$\Delta_{stat} = W/k.$$

Using this simplification, the above equation becomes

$$\Delta_{max} = \Delta_{stat} + [\Delta_{stat}^2 + 2\Delta_{stat}h]^{1/2} \qquad (2.2.3)$$

Once Δ_{max} is computed, the maximum force applied to the spring can be determined from

$$F_{max} = k\Delta_{max} \qquad (2.2.4)$$

It should be realized, however, that this force and associated displacement occur only at an instant. Provided the brock of the sample does not rebound off the spring, it will continue to vibrate until the motion dampens out and the it assumes the static position, Δ_{stat}. Note also that if the brock is held just above the spring,h=0,and dropped ,then the maximum displacement of the block,

$\Delta_{max}=2\Delta_{stat}$ (2.2.5)

In other words, when the block is dropped from the top of the spring or dynamically applied load, the displacement is twice what it would be if it were set on the spring or statically applied load. Here a known weight (block) is dropped onto a post or beam, causing it to deform a maximum amount Δ_{max}. The energy of the falling block is transformed momentarily into axial strain energy in the post and bending strain energy in the beam. Although vibrations are established in each member after impact, they will tend to dissipate as time passes. In order to determine the deformation Δ_{max}, we could use the same approach as the block-spring system, and that is to write the conservation-of-energy equation for the block and post or block and beam of magnetic materials, and then solve for Δ_{max} . However, we can also solve these problems in a more direct manner by modeling the post and beam by an equivalent spring. For example, if a force P displaces the top of the post $\Delta = PL/AE$, then a spring having a stiffness $k = AE/L$ would be displaced the same amount by P, that is, $\Delta = Plk$. In a similar manner, a force P applied to the center of a simply supported beam displaces the center $\Delta = PL^3/48EI$, and therefore an equivalent spring would have a stiffness of $k = 48EI/L^3$. It is not necessary, however, to actually find the equivalent spring stiffness to apply. All that is needed to determine the dynamic displacement, Δ_{max} is to calculate the static displacement, Δ_{stat}, due to the weight W of the block resting on the member. Once Δ_{max} is determined, the maximum dynamic force can then be calculated from $P_{max} = k\,\Delta_{max}$ .If we consider P_{max} to be an equivalent static load then the maximum stress in the member can be determined using statics and the theory of mechanics of materials. Recall that this stress acts only for an instant. In reality, vi brational waves pass through the material, and the stress in the post or the beam, for example, does not remain constant, the impact factor, n. Since $P_{max} = k\,\Delta_{max}$ and $W = k\Delta_{stat}$, then, we can express it as

$$n = 1 + \{1+2(h/\Delta_{stat})\}^{1/2} \qquad (2.2.6)$$

This factor represents the magnification of a statically applied load so that it can be treated dynamically. Using this equation, n can be computed for any member that has a linear relationship between load and deflection. For a complicated system of connected members, however, impact factors are determined by experience or by experimental testing. Once n is determined, the dynamic stress and deflections are easily found from the static stress σ_{stat} and static deflection Δ_{stat} caused by the load W, that is,

$\sigma_{max}=n\sigma_{stat}$ and $\Delta_{max} = n\Delta_{stat}$. (2.2.7)

2.3.1. Experimental results of DA due to impact loading

The experiment of DA due to impact loading was carried out on basis of the above discussion. The strong relation between impact loading and DA is obtained as shown in Fig.2.3.1. Detailed analysis will be reported somewhere in a near future.

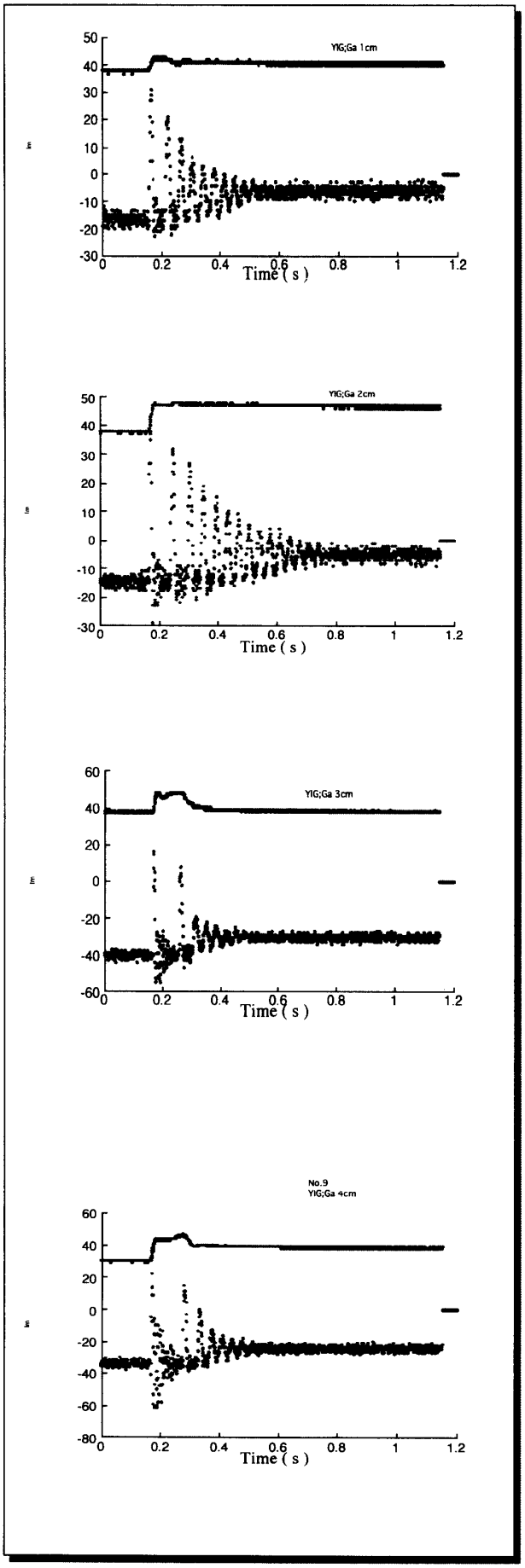

Fig.2.3.1 Hight-dependence of permeability jump on impact loading at room temperature in YIG single crystal; which shows DA at room temperature. The upper curves in each figure indicate the jump of permeability on loading from the hight 1cm, 2cm, 3 cm and 4 cm top. Oscillatory damping curves shown in each figure indicate the signal detected by the strain guage. It should be noted that the knick of permeability curve corresponds to the oscillation peak.

Acknowledgments

The author (K.H) would like to thank Professor K. Shinagawa, Professor A.Braginski and Professor A.Yanase for valuable discussions. The present work was partly supported by a Grant-in Aid for Scientific Research from the Ministry of Eucation, Science and Culture.

References

[1]R.W.Teal and D.W.Temple, Phys. Rev. Lett. 19, 904 (1967).

[2]U.Enz, R.Metselaar and P.J.Rijnierse, J. Phys., 32C1, 703 (1971).

[3]I.Matsubara, K.Hisatake, K.Maeda, Y.Kawai, K. Uematsu, J. Magn. Mag. Mat.104, 427(1992).

[4]M.Pardavi-Horvath, P.E.Wigen and G.Vertesy, J. Appl. Phys., 63, 3110(1988).

[5]M.Pardavi-Horvath, P.E.Wigen and G.Vertesy, J. Appl. Phys., 63, 3107(1988).

[6] S.Chikazumi "Physics of Ferromagnetism 2nd Ed." (Clarendon Press, Oxford, 1997)

[7] K.Ohta,"Zikikougaku no Kiso (Kyouritu Pub. Tokyo,1983)

[8] F.Seitz,"Modern Theory of Solids " (Jone -Wiley,1940)

[9] Y. Shinozuka, Materials Science Forum 83-87, 527 (1992).

[10] I.Song and R. T. Williams, Self-Trapped Excitons (Springer-Verlag, Berlin, 1993).

[11] K.Sato,Biennial Report1999/2000.

[12]S. Nakajima, Y. Toyozawa and R. Abe, "The Physics of Elellrentary Excitations" (Springer-Verlag, Berlin, 1983)

[13] D. V. Lang and R. A. Logan, Phys. Rev. Lett. 39, 635 (1977).

[14] D. J. Chadi and K. J. Chang, Phys. Rev. Lett. 61, 873 (1988).

[15] K. Hisatake, I.Matsubara, K.Maeda, H.Yasuoka,T.Mazaki,T.Miyazaki, S.Kainuma, J. de. Phys., 8, 367 (1998).

[16] J.C.PhilipsPhysics of Hufg TcSuperconductors(Academic Orland,FL,19899.

[17] E. H. de Leeuw, J.Appl.Phys, 45, 3106 (1974).

Appendix I

A part of letter from the late Dr.S.N.Lyakhimets (Theoretical Physicist, Institure of Metals,Kiev,Ukraine) supporting to our migration of oxygen-vacancy model.(1994)

"The positions of levels, corresponding to one- and two charged oxigen vacancies were shown in the band picture.

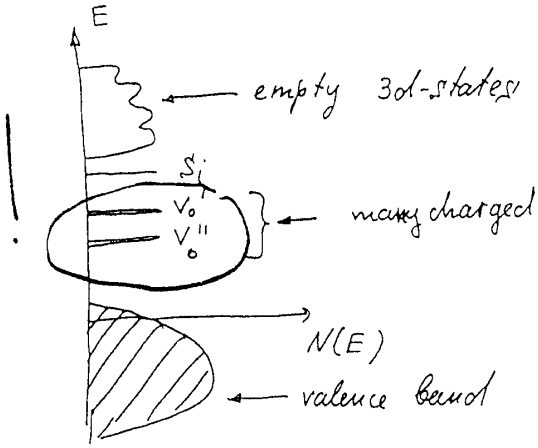

Of course, it should be recharging of these levels at irradiation. Of course, the vacancy mobility should be dependent on the charge state. It should be also interection with magnetic subsystem (spins), therefore, the levels position of vacancy is depend on magnetization orientation. inside gap

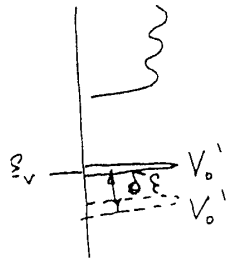

$$\varepsilon_v(\vec{m})$$

$$\delta\varepsilon = \frac{\partial \varepsilon_v(\vec{m})}{\partial \vec{m}} \cdot \delta\vec{m}$$

$\delta\vec{m}$ is magnetization variation.

I think that such band picture does not contradict to your ideas and to your picture of lattice relaxation. I suggest to add, after some

Appendix II

We hope this work help to develope the new solid state physics or new excited materials as illustrated in this figure.